Strange meson production in Al+Al collisions at 1.9 A GeV

Gasik, P.; Piasecki, K.; Herrmann, N.; Leifels, Y.; Matulewicz, T.; Andronic, A.; Averbeck, R.; Barret, V.; Basrak, Z.; Bastid, N.; Benabderrahmane, M. L.; Berger, M.; Buehler, P.; Cargnelli, M.; Caplar, R.; Crochet, P.; Czerwiakowa, O.; Deppner, I.; Dupieux, P.; Dzelalija, M.; Fabbietti, L.; Fodor, Z.; Gasparic, I.; Grishkin, Y.; Hartmann, O. N.; Hildenbrand, K. D.; Hong, B.; Kang, T. I.; Kecskemeti, J.; Kim, Y. J.; Kirejczyk, M.; Kis, M.; Koczon, P.; Kotte, R.; Lebedev, A.; Le Fevre, A.; Liu, J. L.; Lopez, X.; Manko, V.; Marton, J.; Münzer, R.; Petrovici, M.; Rami, F.; Reischl, A.; Reisdorf, W.; Ryu, M. S.; Schmidt, P.; Schüttauf, A.; Seres, Z.; Sikora, B.; Sim, K. S.; Simion, V.; Siwek-Wilczynska, K.; Smolyankin, V.; Suzuki, K.; Tyminski, Z.; Wagner, P.; Weber, I.; Widmann, E.; Wisniewski, K.; Xiao, Z. G.; Yushmanov, I.; Zhang, Y.; Zhilin, A.; Zinyuk, V.; Zmeskal, J.;

Originally published:

June 2016

European Physical Journal A 52(2016), 177

DOI: https://doi.org/10.1140/epja/i2016-16177-y

Strange meson production in Al+Al collisions at 1.9A GeV

P. Gasik[1,2,3], K. Piasecki[1], N. Herrmann[4], Y. Leifels[5], T. Matulewicz[1], A. Andronic[5], R. Averbeck[5], V. Barret[6], Z. Basrak[7], N. Bastid[6], M.L. Benabderrahmane[4], M. Berger[3], P. Buehler[8], M. Cargnelli[8], R. Čaplar[7], P. Crochet[6], O. Czerwiakowa[1], I. Deppner[4], P. Dupieux[6], M. Dželalija[9], L. Fabbietti[2,3], Z. Fodor[10], I. Gašparić[7], Y. Grishkin[11], O.N. Hartmann[5], K.D. Hildenbrand[5], B. Hong[12], T.I. Kang[5,12], J. Kecskemeti[10], Y.J. Kim[5], M. Kirejczyk[1,13], M. Kiš[5,7], P. Koczon[5], R. Kotte[14], A. Lebedev[11], A. Le Fèvre[5], J.L. Liu[15], X. Lopez[6], V. Manko[16], J. Marton[8], R. Münzer[2,3], M. Petrovici[17], F. Rami[18], A. Reischl[4], W. Reisdorf[5], M.S. Ryu[12], P. Schmidt[8], A. Schüttauf[5], Z. Seres[10], B. Sikora[1], K.S. Sim[12], V. Simion[17], K. Siwek-Wilczyńska[1], V. Smolyankin[11], K. Suzuki[8], Z. Tymiński[4], P. Wagner[18], I. Weber[9], E. Widmann[8], K. Wiśniewski[1,4], Z.G. Xiao[19], I. Yushmanov[16], Y. Zhang[4,20], A. Zhilin[11], V. Zinyuk[4], and J. Zmeskal[8]

[1] Institute of Experimental Physics, Faculty of Physics, University of Warsaw, Warsaw, Poland
[2] Excellence Cluster 'Origin and Structure of the Universe', Garching, Germany
[3] Physik Department E62, Technische Universität München, Garching, Germany
[4] Physikalisches Institut der Universität Heidelberg, Heidelberg, Germany
[5] GSI Helmholtzzentrum für Schwerionenforschung GmbH, Darmstadt, Germany
[6] Laboratoire de Physique Corpusculaire, IN2P3/CNRS, and Université Blaise Pascal, Clermont-Ferrand, France
[7] Ruđer Bošković Institute, Zagreb, Croatia
[8] Stefan-Meyer-Institut für subatomare Physik, Österreichische Akademie der Wissenschaften, Wien, Austria
[9] University of Split, Split, Croatia
[10] Wigner RCP, RMKI, Budapest, Hungary
[11] Institute for Theoretical and Experimental Physics, Moscow, Russia
[12] Korea University, Seoul, Korea
[13] National Centre for Nuclear Research, Otwock-Świerk, Poland
[14] Institut für Strahlenphysik, Helmholtz-Zentrum Dresden-Rossendorf, Dresden, Germany
[15] Harbin Institute of Technology, Harbin, China
[16] National Research Centre 'Kurchatov Institute', Moscow, Russia
[17] Institute for Nuclear Physics and Engineering, Bucharest, Romania
[18] Institut Pluridisciplinaire Hubert Curien and Université de Strasbourg, Strasbourg, France
[19] Department of Physics, Tsinghua University, Beijing, China
[20] Institute of Modern Physics, Chinese Academy of Sciences, Lanzhou, China

Abstract. The production of K^+, K^- and $\phi(1020)$ mesons is studied in Al+Al collisions at a beam energy of 1.9A GeV which is close to or below the production threshold in NN reactions. Inverse slopes, anisotropy parameters, and total emission yields of $K^\pm$ mesons are obtained. A comparison of the ratio of kinetic energy distributions of K^- and K^+ mesons to the HSD transport model calculations suggests that the inclusion of the in-medium modifications of kaon properties is necessary to reproduce the ratio. The inverse slope and total yield of ϕ mesons are deduced. The contribution to K^- production from ϕ meson decays is found to be $\left[17 \pm 3(\mathrm{stat})^{+2}_{-9}(\mathrm{syst})\right]$ %. The results are in line with the previous $K^\pm$ and ϕ data obtained for different colliding systems at similar incident beam energies.

PACS. 25.75.Dw Particle and resonance production – 13.60.Le Meson production

1 Motivation

Strange particles are very sensitive probes of hot and dense nuclear matter formed in relativistic nucleus-nucleus collisions. It is predicted that the kaon-nucleon (KN) interaction is modified in dense nuclear matter with respect to the one in vacuum [1,2,3,4,5,6]. Kaons (K^+ and K^0) are subject to a repulsive potential, whereas antikaons (K^- and $\overline{K}^0$) are attracted in a dense nuclear medium. As a result of the in-medium KN interaction the effective mass of kaon, and the threshold energy for its production should increase, whereas for antikaons the corresponding values should decrease substantially [7]. The in-medium modifications of kaonic properties have been already studied experimentally and reported by several experiments focused on strangeness production at near-threshold energies [8,9, 10,11,12]. Conclusions were based on the comparison to the results of theoretical transport models.

For decisive conclusions on in-medium modifications, one has to account for feeding of the K^- emission by the $\phi(1020)$ meson decays, since the $\phi(1020)$ is decaying into a K^+K^- pair with a probability of 48.9 %. A comparison of the mean free path of $\phi(1020)$ mesons, $c\tau_\phi \approx 50$ fm, to the average duration of the hot and dense collision zone (20–30 fm/c [6]) suggests that most of ϕ mesons decay outside this zone. It should be also noted that the ϕ meson mass is only 32 MeV/c^2 larger than that of a K^+K^- pair. As a result, K^- originating from the ϕ meson decays are governed by different kinematics than those emitted directly from the collision zone. It is therefore crucial to find out in the first step the relative contributions of these sources to the total K^- production.

It has been reported for two systems, Ni+Ni and Ar+KCl, colliding at beam kinetic energies of 1.7–1.9A GeV, that about 20% of the K^- mesons originate from ϕ meson decays [13,14,15]. Here, we present a third data point on this subject, supporting the statement that ϕ meson decays are a relevant source of the K^- mesons in heavy-ion collision at energies below the NN production threshold. We also propose a simple two-source model that aims to reconstruct the kinematic properties of direct kaons from the inclusive K^- spectra.

2 FOPI spectrometer

FOPI is a modular spectrometer for fixed-target experiments at the SIS-18 synchrotron in the GSI, Darmstadt. The FOPI set-up consists out of 4 subdetectors. Two drift chambers are mounted around the target, CDC (Central Drift Chamber) and Helitron. The CDC detector spans a wide range of polar angles $27° < \vartheta_{\rm lab} < 113°$. It is surrounded by a Plastic Scintillation Barrel, a time-of-flight (ToF) detector covering polar angles $27° < \vartheta_{\rm lab} < 57°$. These detectors are located inside the magnet solenoid with a magnetic field of 0.6 T. The PlaWa (Plastic Scintillation Wall) detector is installed at the forward directions behind the Helitron, outside the magnetic field. The target is shifted 40 cm upstream with respect to the nominal position.

A particle moving inside the magnetic solenoid follows the path of a helix. If it passes through the CDC, electric signals are induced on the sense wires (dubbed below "hits") which are digitized by a Flash-ADC system. A fast on-line algorithm extracts the characteristics of the signals (time with respect to the event start, amplitude, and length). An off-line procedure uses this information to obtain the drift time, energy loss, and position of a hit. Particle tracks are reconstructed by employing the tracking algorithm based on a local approach searching for consecutive hits on a circle (straight line) in the plane transverse (longitudinal) to the beam axis.

Particle identification in the CDC is obtained by correlating the energy loss $\mathrm{d}E/\mathrm{d}x$ and the curvature of a track. Particle masses extracted from this procedure shall be dubbed $m_{\rm CDC}$. Plastic detectors, together with the Start counter placed about 2 meters in front of the target, yield an additional ToF measurement of a particle. For a CDC track, which can be matched with a hit in the ToF Barrel (or PlaWa), the particle type is identified by employing the relativistic relation between momentum and velocity, $p = m\beta\gamma$, where m is the mass of a particle, β its reduced velocity v/c, and γ is the Lorentz factor. The mass obtained by this procedure shall be dubbed $m_{\rm Bar}$. The timing resolution of the plastic detector is crucial and limits the extension of the momentum space, for which the charged kaons can be identified. More details on the configuration of FOPI submodules and their performance can be found in refs. [16,17].

3 Data analysis

3.1 Al+Al experiment

The aluminium target of 567 mg/cm^2 thickness was irradiated by the beam of aluminium ions with an intensity

Send offprint requests to:

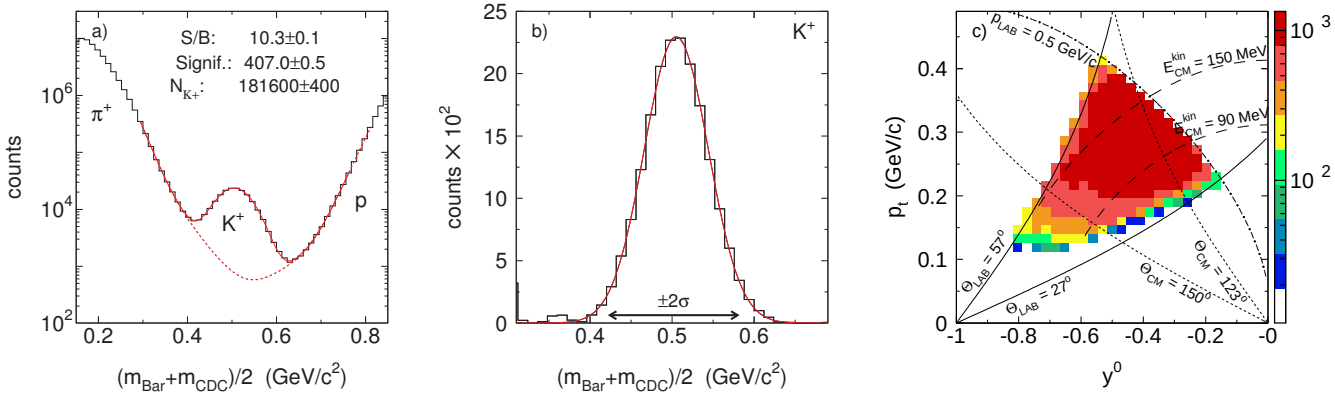

Fig. 1. a) Experimental mass distribution of positively charged particles with momentum $p < 0.5$ GeV/c. The K^+ signal is seen between the π^+ and proton signals. Solid (dotted) curve represent the signal (background) components of the function fitted to the distribution. b) K^+ signal after background subtraction. The red curve represents the Gaussian fit. c) Phase space distribution of the reconstructed K^+ mesons. Solid and dashed-dotted lines depict the angular and momentum limits of the detector, respectively. Dashed (dotted) lines represent the constant values of kinetic energy (polar angle) in the center-of-mass frame. See text for details.

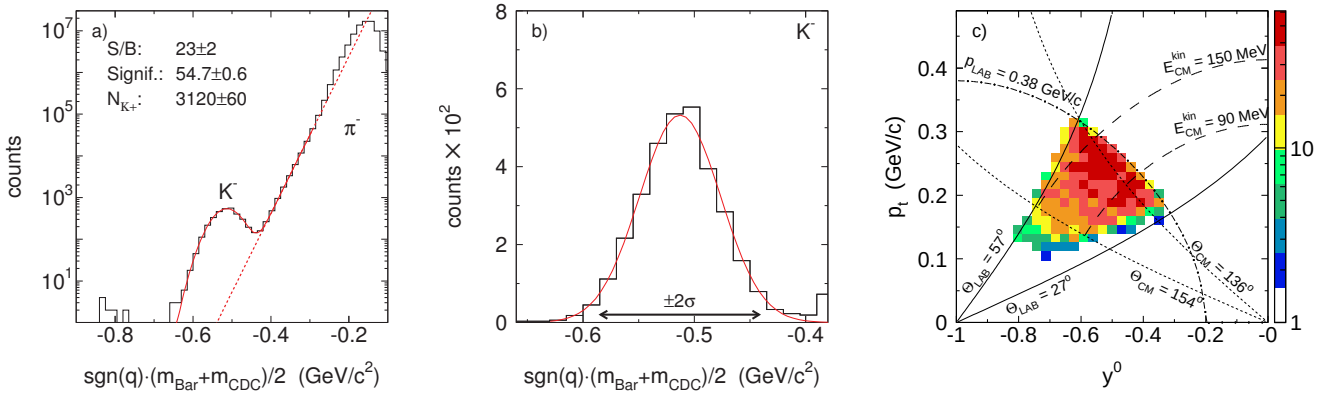

Fig. 2. a) Experimental mass distribution of negatively charged particles with momentum $p < 0.38$ GeV/c. The K^- signal is seen on the tail of the pion signal. Solid (dotted) curve represent the signal (background) components of the function fitted to the distribution. b) K^- signal after the background subtraction. The red curve represents the Gaussian fit. c) Phase space distribution of the reconstructed K^- mesons. Solid and dashed-dotted lines depict the angular and momentum limits of the detector, respectively. Dashed (dotted) lines correspond to the constant values of kinetic energy (polar angle) in the center-of-mass frame. See text for details.

of 8×10^5 s^{-1} at the kinetic energy of 1.9A GeV. The collision centrality was determined by the multiplicity of charged particles in the ToF Barrel and PlaWa detectors. A minimum multiplicity in the Plastic Wall detector was required as a trigger condition to select the more central events. The number of collected events is 1.59×10^8. The results reported in this paper are obtained for the most central 9% of the total geometrical cross section ($\Delta\sigma \approx 140$ mb). Using a geometrical *sharp cut-off* model, one can estimate the maximal value of impact parameter b for the analysed data sample to be ∼2.1 fm. The mean number of participant nucleons was calculated using the *participant-spectator* model described in [18], and is found to be $\langle A_{\rm part}\rangle_{\rm b} \approx 42$.

3.2 Kaon identification

K^+ and K^- mesons were identified by the CDC tracks matched with the hits in the ToF Barrel. Figs. 1a and 2a present the experimental mass distributions around $m_{K^\pm}$ of positively (negatively) charged particles with momenta $p < 0.5$ (0.38) GeV/c, respectively.

The K^+ signal, concentrated around 0.5 GeV/c^2, is situated on the tails of the proton and π^+ signals, which can be described by a combination of Gaussian and exponen-

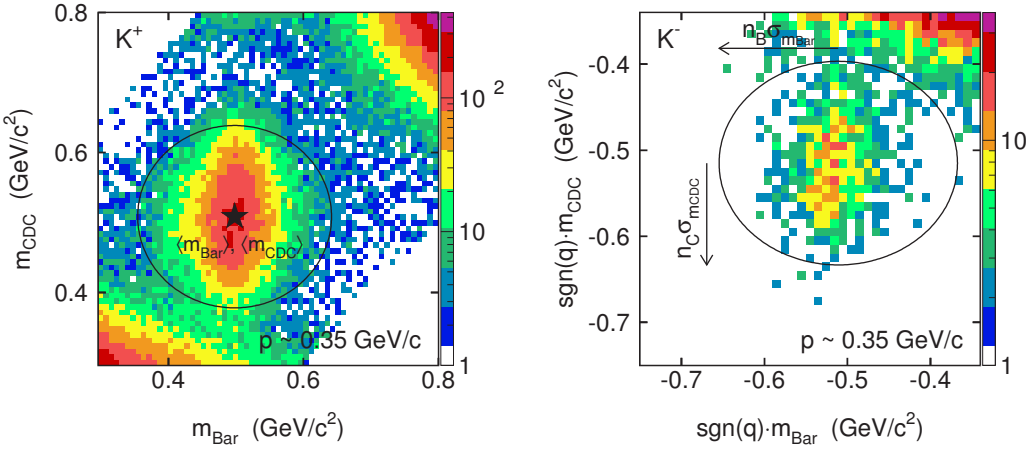

Fig. 3. Correlation plot of m_{Bar}–m_{CDC} mass distributions of particles with momentum $p \approx 0.35$ GeV/c^2, shown around the nominal masses of K^+ (left panel) and K^- (right panel) mesons. Ellipses represent the cuts imposed for the ϕ meson identification.

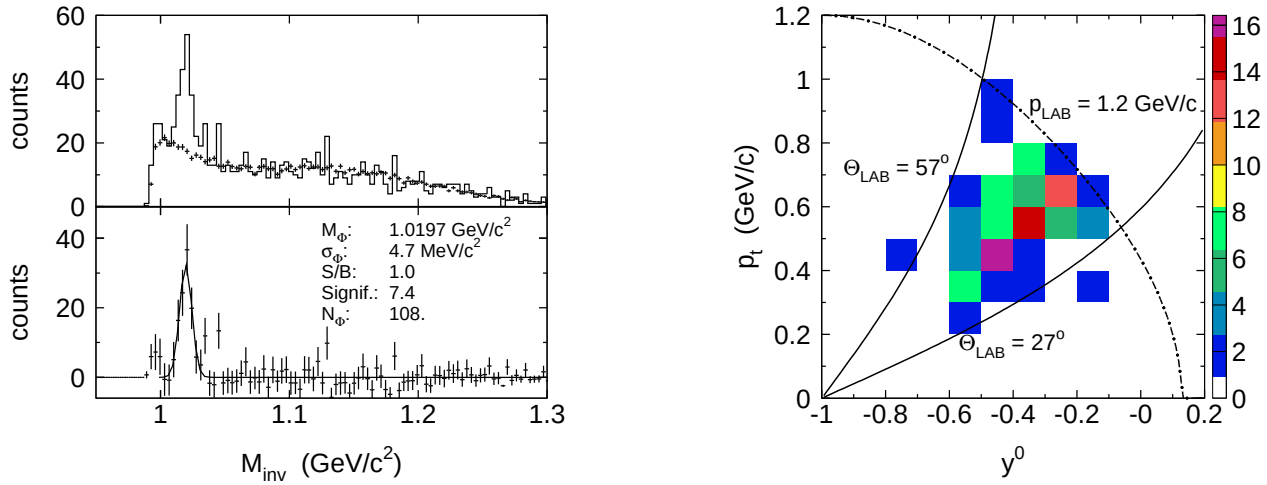

Fig. 4. Left, upper panel: Invariant mass distribution of K^+K^- pairs. The background spectrum of uncorrelated pairs is shown by the crosses. Left, lower panel: The ϕ meson signal after the background subtraction, fitted with a Gaussian function (solid curve). Right: $p_{\mathrm{t}} - y^0$ phase space distribution of identified ϕ mesons. Solid lines depict the angular limits of the detector and the dashed-dotted line - the momentum cut.

tial functions (dotted line). The background under the K^- peak is caused by the π^- mesons, and can be described by an exponential function.

In order to enhance the signal-to-background ratio, and the significance of the signal, the following set of cuts was applied:

- a limit on the K^+ (K^-) momentum to $p_{\mathrm{lab}} < 0.5$ (0.38) GeV/c, to reduce the contamination from pions and protons;
- a cut on the transverse momentum ($p_{\mathrm{t}} > 0.1$ GeV/c), to reject particles spiralling in the CDC;
- cuts on the distance of closest approach between the track and the collision vertex in the transverse plane ($d_0 < 1$ cm) and its uncertainty ($\sigma_{\mathrm{d_0}} < 0.14$ cm), to suppress decay products outside the target;
- a condition on the minimum number of hits on a track in the CDC (35 for K^+ and 40 for K^-) for the higher quality of the reconstructed tracks;
- a cut on the angular difference between the extrapolation of the CDC track and the matched ToF Barrel hit, $\Delta\phi < 5°$.

After background subtraction, clear peaks around the nominal $K^{\pm}$ mass are seen in figs. 1b and 2b. The solid curves represent the Gaussian fits. Within a $\pm 2\sigma$ region around the maximum of the fitted function (as indicated in the figs. 1b and 2b) about 180×10^3 K^+ and 3×10^3 K^-

mesons were reconstructed in the analysed data sample with a signal-to-background ratio S/B of 10 (K^+) and 23 (K^-), and a significance (defined as $S/\sqrt{S+B}$) of 407 and 55 for K^+, and K^- mesons respectively. The acceptance ranges for K^+, and K^- mesons are shown in figs. 1c and 2c in terms of transverse momentum p_t, and normalised rapidity y^0, where $y^0 = y_{lab}/y_{NN} - 1$ is defined to be +1 (-1) at projectile (target) rapidity, and $y_{NN} \approx 0.89$.

The systematic uncertainties of the integrated background were estimated by varying the function fit parameters. They are found to be at the level of 40% (K^+) and 20% (K^-). Note, that the corresponding signals are strong enough for the influence of the above-mentioned errors to be minor.

In order to estimate the systematic uncertainties associated with the cutting strategy, apart from the "standard" set of cuts, "narrow" and "wide" cut sets were applied to the parameters used for enhancing the quality of the tracks and the matching of CDC with Plastic Barrel hits. In case of the "narrow" cuts the background is minimised but at the same time the statistics of identified particles is reduced. The "wide" cuts are less restrictive. This results in an increase of the background but does not lead to a signal increase at the same level.

In all the sets of cuts used in the charged kaons analysis, the total and transverse momentum cut were kept constant.

3.3 ϕ(1020) identification

Identification of ϕ mesons is possible via their charged decay in the FOPI spectrometer: $\phi \rightarrow K^+K^-$. The branching ratio for this channel is $\Gamma_{K^+K^-}/\Gamma = 48.9 \pm 0.5\,\%$ [19]. Hence, ϕ mesons can be identified by an invariant mass analysis of K^+K^- pairs. Due to the short lifetime of ϕ mesons ($c\tau \approx 1.55 \times 10^{-22}$ s) it is not possible to disentangle its decay vertex from the collision vertex.

In order to increase the identified ϕ meson signal, the maximum momentum conditions were increased for this analysis to $p_{lab} < 0.6\,\mathrm{GeV}/c$. However, such an increase may result in an inclusion of some non-kaons ($\pi^\pm$, protons) in the sample of kaon pairs. To reduce such a side effect, a geometrical (2D-ellipse) cut on the mass of K^+ and K^- mesons was applied, as shown in fig. 3.

For the further ϕ analysis, only the kaons fulfilling the following ellipse equations were chosen:

$$\left(\frac{m_{Bar} - \langle m_{Bar}\rangle}{n_B \sigma_{m_{Bar}}}\right)^2 + \left(\frac{m_{CDC} - \langle m_{CDC}\rangle}{n_C \sigma_{m_{CDC}}}\right)^2 < 1 \quad , \quad (1)$$

where m_{Bar}, m_{CDC} are the mass parameters (see sec. 2), n_B, n_C are the factors defining widths of the mass cuts for kaons, $\langle m_{Bar}\rangle$, $\langle m_{CDC}\rangle$ are the mass parameter mean values, and $\sigma_{m_{Bar}}$, $\sigma_{m_{CDC}}$ are the dispersions of the kaon mass distributions. The values of four latter parameters are momentum- and charge-dependent. The widths of ellipses given by $n_B = 4.5$ and $n_C = 2$, were chosen for the further analysis. An influence of the cut on the systematic uncertainty of the ϕ meson yield was estimated by varying these values.

Fig. 4 shows the invariant mass plot of ϕ mesons reconstructed in the CDC+Barrel subsystem with a clear indication of a peak close to the nominal $\phi(1020)$ mass.

The combinatorial background was reconstructed using the event-mixing method, where matched kaons were selected from different events. In order to bring the kinematic conditions of mixed pairs close to those of true ones, two conditions were imposed:

- K^+ were selected from events exhibiting at least one K^-,
- The CDC hit multiplicity distribution, correlated with the collision centrality, was divided into 8 groups (centrality classes). Kaons were matched from events attributed to the same centrality class.

The background distribution was adjusted to the one of true pairs by normalising the spectrum to the latter one in the region $M_{inv} > 1.05$ GeV/c. The resulting combinatorial background spectrum is indicated with crosses in fig. 4 (upper left panel). 108 ϕ mesons were reconstructed within $\pm 2\sigma$ range around the centre of the fitted Gaussian function, which is shown as full line in fig. 4 (lower left panel). The distribution of reconstructed ϕ mesons in the p_t versus y^0 plane is shown in the right panel of fig. 4. In order to extract the ϕ meson yield, the efficiency of the detector was deduced using the GEANT package (see sec. 3.4.2).

3.4 Efficiency correction

Simulations of the detection efficiency of $K^\pm$ and ϕ mesons were performed in the framework of the GEANT [20] environment. Single K^+, K^- or ϕ mesons were added to events of Al+Al collisions generated by the IQMD model [21],

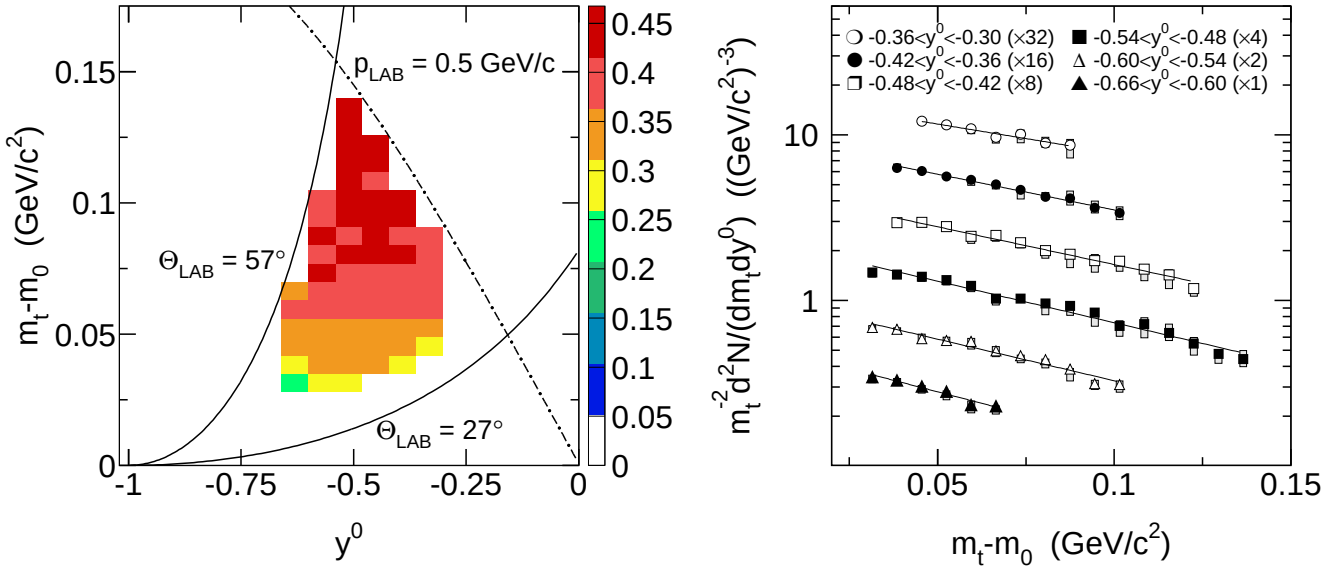

Fig. 5. Left: efficiency of the K^+ meson identification for the different bins of $m_t - m_0$ and y^0 used for the transverse mass spectra analysis (see sec. 3.4.1 for more details). Right: transverse mass spectra of K^+ mesons. The spectra measured in different slices of normalised rapidity are multiplied by the subsequent powers of two. Solid lines indicate the Boltzmann function fits. Shaded rectangles correspond to the systematic uncertainties.

which served as a realistic background for tracking and PID. All particles of the combined event were tracked and digitised within GEANT, and subsequently reconstructed by the same off-line algorithms as that used for the experimental data.

3.4.1 K^+ and K^- mesons

Charged kaons were generated from a uniform $p_t - y^0$ distribution, and each $K^\pm$ meson was subsequently added to the collection of particles in an event generated by the IQMD code. In total, 6.5×10^6 events were simulated. For each studied kinematical distribution, which would be used further in sec. 4), a corresponding efficiency map was evaluated. It allowed for correcting these spectra on a bin-by-bin basis.

As an example, the distribution of the K^+ meson efficiency as a function of transverse mass m_t and normalised rapidity y^0 is shown in the left panel of fig. 5. The covered phase space region reflects the acceptance of the CDC+Barrel detectors.

To check whether the choice of the primary distribution of charged kaons influences the efficiency map and thus the final results, $K^\pm$ mesons were also sampled from a Boltzmann-like distribution multiplied by the angular anisotropy term:

$$\frac{\mathrm{d}^2N}{\mathrm{d}E^{\mathrm{kin}}_{\mathrm{CM}}\mathrm{d}\cos\vartheta_{\mathrm{CM}}} = N_0 \cdot p_{\mathrm{CM}} E_{\mathrm{CM}} \exp(-E_{\mathrm{CM}}/T_{\mathrm{eff}}) \cdot (1 + a_2 \cos^2\vartheta_{\mathrm{CM}}) \quad , \tag{2}$$

where N_0 is the overall normalisation factor, E_{CM} and p_{CM} are the energy and momentum of a particle in the center-of-mass frame, T_{eff} is the inverse slope parameter ("effective temperature" of a particle source), and a_2 is the coefficient quantifying the degree of asymmetry (in the CM frame). For the K^+ efficiency estimation a_2 was set to 0.3, and T_{eff} to 100 MeV. The observed differences were found to be negligible ($< 2\%$) and had no influence on the systematic uncertainty of the final results.

3.4.2 Efficiency of ϕ reconstruction

For the evaluation of the reconstruction efficiency ϕ mesons were generated according to the isotropic ($a_2 = 0$) Boltzmann-like function (c.f. eq. (2)), and added to the IQMD events ($\sim 6 \times 10^5$ events were simulated in total). Since the precise kinematic properties of ϕ meson are unknown, the T_{eff} parameter was varied within [80, 130] MeV. The influence of these variations on the final results was included in the respective systematic errors. As all the simulations were performed in the $\phi \to K^+K^-$ channel, the efficiency values presented below will be given as normalised with respect

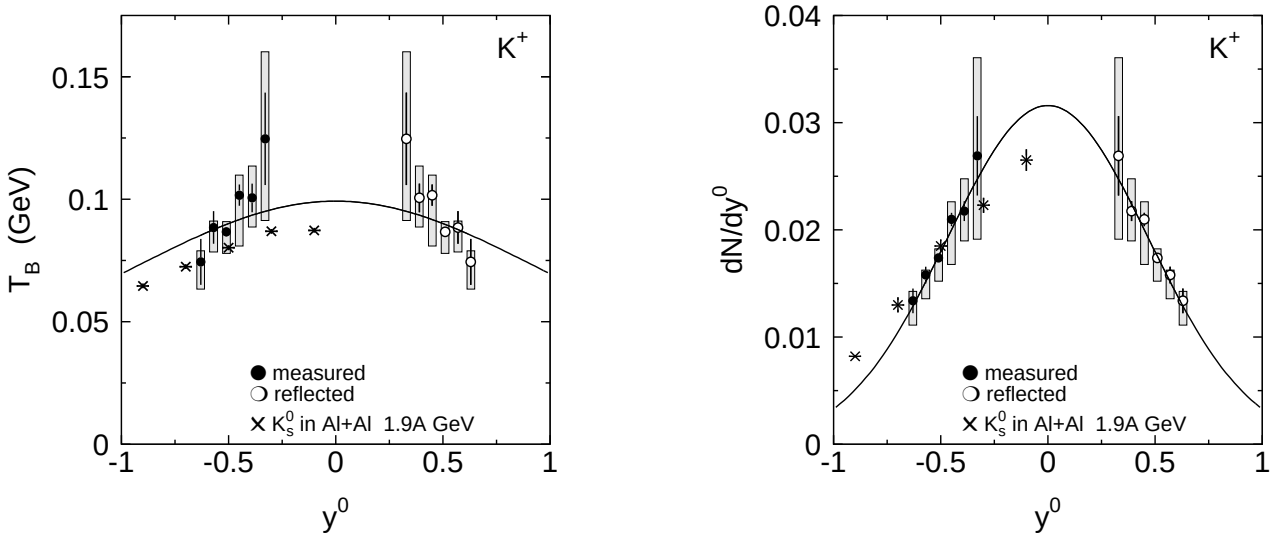

Fig. 6. Left: inverse slope parameters ($T_{\rm B}$) of the transverse mass spectra of K^+ mesons as a function of the normalised rapidity. Solid line represents the fit of function (6). Right: rapidity density distribution for K^+. The solid curve represents the Gaussian fit to the data. Crosses depict the respective emission patterns of K^0_s from the same experiment [24]. The experimental results (full circles) were reflected (hollow circles) due to the symmetry of the colliding system. The vertical bars and shaded rectangles correspond to the statistical and systematic uncertainties, respectively.

to this channel. However, for the final results reported in sec. 5, the branching ratio of this decay mode will be included. The efficiency analysis presented below was performed for the "standard" set of track quality cuts, however, both "narrow" and "wide" sets were used to evaluate the systematic uncertainties (see sec. 3.2 for more details).

For more thorough understanding of the ϕ meson detection losses, the total efficiency ($\epsilon_{\rm tot}$) was split into two terms (see eq. 6 in [22]):

$$\epsilon_{\rm tot} = \epsilon_{\rm max} \cdot \epsilon_{\rm det} \quad . \tag{3}$$

$\epsilon_{\rm max}$ is the efficiency of detection of ϕ mesons in the K^+K^- channel by the ideal apparatus and includes losses due to the geometrical acceptance, decays of kaons on their path towards ToF Barrel, and the limitation of momenta of kaons to 0.6 GeV/c. $\epsilon_{\rm det}$ corresponds to the subsequent loss of ϕ meson signal due to the internal efficiency of the CDC+ToF Barrel subsystem, including the limitations due to measurement capabilities, tracking, matching quality, and the PID algorithm.

The same momentum cuts were applied in the efficiency evaluation procedure as for the experimental data. Table 1 reports both the factors and the total efficiency for different temperatures of the ϕ meson sources. As expected, the $\epsilon_{\rm det}$ was found to be independent within the 1σ uncertainty of properties of the distribution of primary ϕ mesons. Regarding $\epsilon_{\rm max}$, in the analysis presented in [22] the variations of this parameter due to different temperatures of the ϕ meson source reached a factor of 4. In contrast, for our analysis $\epsilon_{\rm max}$ was found to be clearly better anchored. This is due to the different acceptance windows available for both experiments. For the Al+Al case shifting the target by 40 cm upstream with respect to its nominal position resulted in moving the phase space coverage towards midrapidity, where the production yield is much greater. The total ϕ meson efficiency was found to be about 0.4 – 0.5 %.

Table 1. Efficiencies for ϕ meson detection in the K^+K^- decay channel for different temperatures of the ϕ emitting source. $\epsilon_{\rm max}$ is the efficiency within the geometrical and momentum limits of an ideal apparatus including the kaon decays on their path toward ToF Barrel, and $\epsilon_{\rm det}$ is the efficiency of the CDC+Barrel detector for kaons reaching the ToF Barrel (see eq. (3)). $\epsilon_{\rm tot}$ is the total detection efficiency.

$T_{\rm eff}$ [MeV]	$\epsilon_{\rm max}$ [%]	$\epsilon_{\rm det}$ [%]	$\epsilon_{\rm tot}$ [%]
80	0.88 ± 0.02	44 ± 2	0.38 ± 0.02
100	0.99 ± 0.02	43 ± 2	0.43 ± 0.02
120	1.03 ± 0.02	47 ± 2	0.48 ± 0.02
130	1.03 ± 0.02	45 ± 2	0.46 ± 0.02

4 Results on the production of charged kaons

4.1 K^+ phase space analysis in the $m_t - y^0$ representation

This section reports on the two-dimensional $m_t - y^0$ analysis of the K^+ phase space distribution, and the calculation of the total emission yield. The same analysis applied to K^- was found to be unstable due to considerably lower statistics.

We start from the Boltzmann-like distribution parametrised in y_{CM} (rapidity of particle in the frame of its source), and transverse mass $m_t = \sqrt{p_t^2 + m_0^2}$ (m_0 is the particle's mass in vacuum),

$$\left.\frac{1}{m_t^2}\frac{d^2N}{dm_t dy_{CM}}\right|_{y_{CM,i}} = A_0(y_{CM}) \cdot e^{-m_t/T_B(y_{CM})} \quad , \quad (4)$$

where A_0 is the normalisation factor, and T_B is the inverse slope. In contrast to the pure Boltzmann approach (cf. Sect. III in [23]), we allow A_0 and T_B to be the free functions of rapidity, which are to be extracted by fitting to the experimental data. In the next step we change the variables to $m_t - m_0$, and y^0. For every i-th slice of y^0,

$$\left.\frac{1}{m_t^2}\frac{d^2N}{d(m_t - m_0)dy^0}\right|_{y_i^0} = A(y_i^0) \cdot e^{-(m_t - m_0)/T_B(y_i^0)} \quad , \quad (5)$$

where $A(y_i^0) = A_0(y_i^0) \cdot y_{NN} \cdot \exp(-m_0/T_B)$. The reconstructed spectra of transverse mass of positively charged kaons within the y^0 range of $(-0.66, -0.36)$ were scaled by $1/m_t^2$, and plotted logarithmically in fig. 5. The systematic errors are shown by the shaded rectangles. They reflect the sensitivity of data to variations of cut parameters in the procedures of kaon track finding, different parameters in the background evaluation procedure, and the uncertainty associated with the adjustment of the centrality class between the experimental and simulated data. The convention for these errors applied throughout the present paper is to cover all the observed range of the data point caused by variations of the above-mentioned parameters. The spectra were then fitted with the eq. 5, and T_B parameters were found. We do not imply the thermalisation of kaons, but use the above-mentioned formula as a suitable representation of the data and the T_B as a measure of hardness of the spectrum.

The rapidity distribution of the slope parameters T_B extracted by the above-mentioned fitting procedure is shown in the left panel of fig. 6. The symmetry of the colliding system allows to reflect the data points with respect to midrapidity. The figure also shows the T_B profile of K_s^0 emitted from the same colliding system [24]. Spectra of positively charged kaons appear to be somewhat harder than those of K_s^0, however, large systematic errors do not exclude that the slopes are identical. The distribution of temperatures as a function of normalised rapidity has been fitted with the prediction of the Boltzmann model of particles emitted isotropically from the thermalised source:

$$T_B(y^0) = \frac{T_{eff}}{\cosh\ (y^0 \cdot y_{NN})} \quad , \quad (6)$$

where the temperature T_{eff} within this model, considered as an overall effective parameter quantifying the hardness of the kaon emission, has been found to be $T_B(K^+) = 99 \pm 2(\text{stat})^{+\ 4}_{-11}(\text{syst})$ MeV.

The distribution of normalised rapidity of K^+ has been obtained by an analytic integration of eq. (5) from 0 to ∞,

$$\left.\frac{dN}{dy^0}\right|_{y_i^0} = A \cdot T_B^3 \cdot \left(\frac{m_0^2}{T_B^2} + 2\frac{m_0}{T_B} + 2\right) \quad . \quad (7)$$

In the evaluation of the statistical error of this formula, the covariance term between A and T_B parameters was included. The resulting dN/dy^0 distribution is shown in fig. 6. In the range of rapidities available for this analysis the profiles for the K^+ and K_s^0 from ref. [24] are found to overlap.

The analysis of the two-dimensional $m_t - y^0$ distribution allows to extrapolate the data from an experimentally available region of phase space, and integrate the distribution to obtain the total yield. However, since the accessible region is partial, the extrapolated value of yield may depend on the model assumptions. The data obtained within the ToF Barrel acceptance window follow a Gaussian profile which is shown by the full line in the right panel of fig. 6. We stress here, that this profile is employed only phenomenologically. A cross-check of this approach by reconstructing the yield using different representation will be presented in the next subsection.

The total K^+ emission yield within this approach is $P_{K^+} = \left[3.72 \pm 0.05(\text{stat})^{+0.28}_{-0.52}(\text{syst})\right] \times 10^{-2}$. Interestingly, the obtained yield is identical within experimental uncertainties to that of K^0, extracted using the same $m_t - y^0$ analysis, although in the considerably wider range of phase space [24].

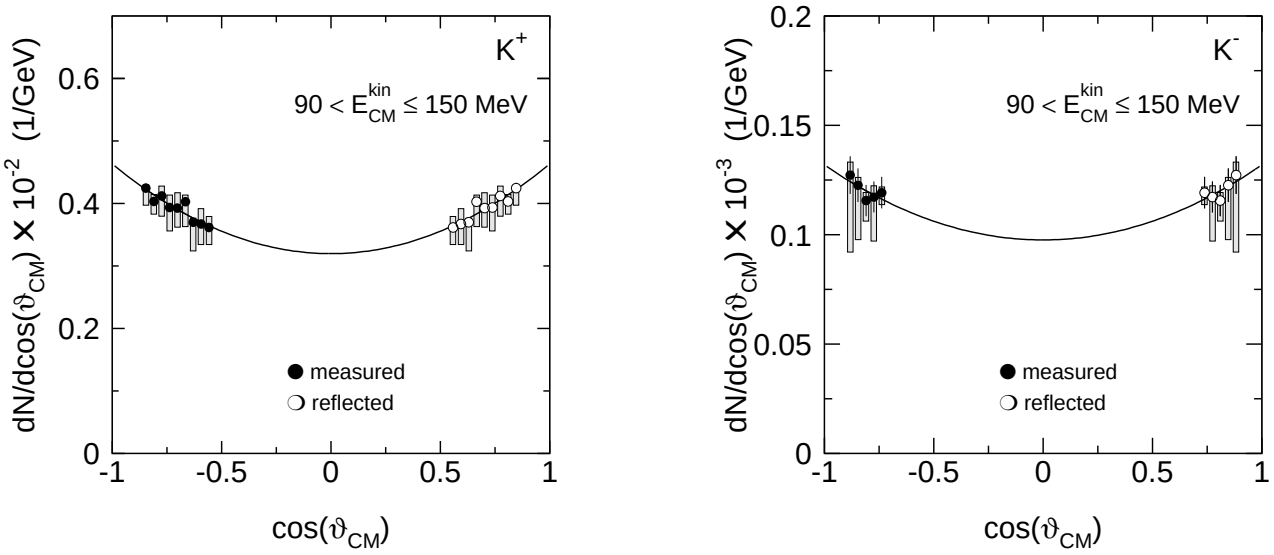

Fig. 7. Angular distribution of positive (left) and negative (right) kaons plotted as a function of $\cos(\vartheta_{\mathrm{CM}})$ for the particles with center-of-mass kinetic energy of $E_{\mathrm{CM}}^{\mathrm{kin}} \in [90, 150]$ MeV. Experimental values are reflected with respect to $\cos\vartheta_{\mathrm{CM}} = 0$. The solid line represents the fit of function (8). Black bars and shaded rectangles correspond to the statistical and systematic uncertainties, respectively.

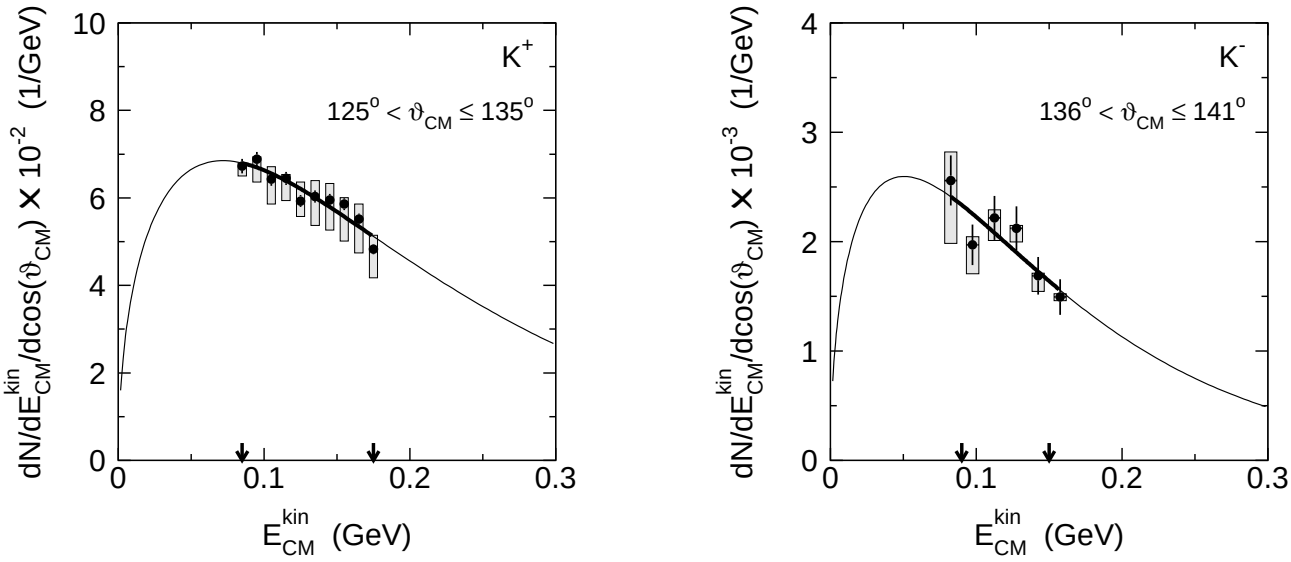

Fig. 8. Kinetic energy distribution of charged kaons in the CM frame obtained for the particles emitted within $\vartheta_{\mathrm{CM}} \in [125°, 135°]$ (K^+) and $\vartheta_{\mathrm{CM}} \in [136°, 141°]$ (K^-). The full line represents the fit of function (10). The black arrows indicate the window used for adjustment of normalisation to eq. (8), see text for details.

4.2 Kinetic energy and polar angle distributions of K^+ and K^-

In this approach it is assumed that the charged kaon emission in the nucleon-nucleon centre of mass can be parametrised by the Boltzmann-like kinetic energy term multiplied by the polar-angular term (c.f. eq. (2)). We only note that in formula (2) the kinetic energy and polar angle are not correlated. This allows to extract the a_2 and T_{eff} parameters independently by projecting data on the $\cos\vartheta_{\mathrm{CM}}$ and $E_{\mathrm{CM}}^{\mathrm{kin}}$ axes, correspondingly. In light of the limited sample of negative kaons, the fact that the total number of projections in this method is smaller than for the $m_{\mathrm{t}} - y^0$ analysis turned out to be crucial for stabilising the K^- results.

The spectra of kinetic energy and polar angle were trimmed to the available phase space (c.f. figs. 1 and 2) in order to minimise the edge effects.

Fig. 7 shows the polar angle distributions of K^+, and K^- emitted with kinetic energies $90 < E_{CM}^{kin} < 150$ MeV, and in the angular range: $123° < \vartheta_{CM} < 150°$ ($136° < \vartheta_{CM} < 154°$) for K^+ (K^-), respectively. The corresponding projection of eq. (2) runs as follows:

$$\left[\frac{dN}{d\cos\vartheta_{CM}}\right]_{E_{k1}..E_{k2}} = B_{E_{k1}..E_{k2}}\cdot(1+a_2\cos^2\vartheta_{CM}) \quad , \quad (8)$$

where $B_{E_{k1}..E_{k2}}$ is the normalisation constant for kaons with kinetic energies in the range $[E_{k1}..E_{k2}]$ (here, [90..150] MeV). A fit of this formula to the angular distributions of K^+ and K^- mesons allowed to extract the respective a_2 coefficients (see Table 2 for all the relevant results of this procedure):

$$\begin{aligned} a_2(K^+) &= 0.45 \pm 0.08(\text{stat})^{+0.18}_{-0.11}(\text{syst}) \\ a_2(K^-) &= 0.35 \pm 0.40(\text{stat})^{+0.11}_{-0.83}(\text{syst}) \end{aligned} \quad . \quad (9)$$

The obtained coefficients were found to be rather small for K^+, and consistent with 0 for K^-, a pattern observed also in the somewhat heavier Ni+Ni system at the same beam energy (see fig. 16b in [9]). Values of $B_{E_{k1}..E_{k2}}$ extracted by the fit procedure are reported in table 2, and will be further used for the evaluation of the total yield.

In the next step, the kaon data in the polar angle ranges of $125° < \vartheta_{CM} < 135°$ (for K^+), and $136° < \vartheta_{CM} < 141°$ (for K^-) were projected to the kinetic energy axis. The resulting E_{CM}^{kin} distributions are shown in fig. 8. The corresponding projection of eq. (2) follows:

$$\left[\frac{dN}{dE_{CM}^{kin}}\right]_{\vartheta_{CM,1}..\vartheta_{CM,2}} = C_{\vartheta_{CM,1}..\vartheta_{CM,2}}\cdot p_{CM}E_{CM}\exp(-E_{CM}/T_{eff}) \quad , \quad (10)$$

where $C_{\vartheta_{CM,1}..\vartheta_{CM,2}}$ is the normalisation constant for kaons emitted in the polar angle range of $[\vartheta_{CM,1}..\vartheta_{CM,2}]$. Fitting the formula above to the experimental data allowed to extract the following inverse slopes:

$$\begin{aligned} T_{eff}(K^+) &= 109 \pm 2(\text{stat})\ ^{+\ 6}_{-13}(\text{syst})\,\text{MeV} \\ T_{eff}(K^-) &= \ \ 82 \pm 6(\text{stat})\ ^{+21}_{-\ 6}(\text{syst})\,\text{MeV} \end{aligned} \quad . \quad (11)$$

These results are in a good agreement with the inverse slopes of charged kaons emitted from Ni+Ni collisions in a similar centrality class ($\langle A_{part}\rangle_b = 34$), both in terms of absolute values and in the superiority of T_{K^+} over T_{K^-} (c.f. figs. 15b and 20 in [9]).

4.3 Total emission yields of K^+ and K^-

In order to obtain the total kaon emission yield from the results reported in sec. 4.2, one has to account for different ranges of scope in the eqs. (8) and (10). Thus, in the first step the integral of eq. (8) was evaluated:

$$I_{E_{k1}..E_{k2}} = \int_{-1}^{1}\left[\frac{dN}{d\cos\vartheta_{CM}}\right]_{E_{k1}..E_{k2}} = 2B_{E_{k1}..E_{k2}}\cdot\left(1+\frac{a_2}{3}\right) \quad . \quad (12)$$

The results are presented in table 2. This integral represents the yield of kaons emitted in the E_{CM}^{kin} range of [90, 150] MeV. Note, that the smaller relative errors of $I_{E_{k1}..E_{k2}}$ compared to those for $B_{E_{k1}..E_{k2}}$ and a_2 fit parameters are due to strong anti-correlation term between the latter parameters. In the next step the normalisation of the kinetic energy spectrum expressed by eq. (10) was adjusted such that the integral of this spectrum in range $E_{CM}^{kin} \in [90, 150]$ MeV was equal to the value of $I_{E_{k1}..E_{k2}}$. Such an adjusted energy spectrum was subsequently integrated to obtain the total yield of charged kaons:

$$\begin{aligned} P_{K^+} &= \left[3.75 \pm 0.07(\text{stat})^{+0.33}_{-0.64}(\text{syst})\right]\times 10^{-2} \\ P_{K^-} &= \left[0.95 \pm 0.10(\text{stat})^{+0.26}_{-0.01}(\text{syst})\right]\times 10^{-3} \end{aligned} \quad . \quad (13)$$

As mentioned above, this method provided a stable value of the K^- yield. The yields of K^+ obtained using this approach, and by the 2-dimensional analysis of the $m_t - y^0$ phase space were found to be consistent. The systematic errors, as for all the other results mentioned above, account for the variations of cutting parameters in the procedures of kaon track finding and background subtraction, and the determination of the collision centrality. They cover all the range of the yield values due to these variations.

In comparison to the charged kaon multiplicities at similar energy and centrality, the obtained yields of K^+ (K^-) were found to be about 1.8 (2.2) times smaller than for kaons emitted in Ni+Ni collisions at $\langle A_{part}\rangle_b = 74$ [25]. They were also found to be about 2.1 (1.4) times larger than for kaons emitted from Ni+Ni at the kinetic energy of 1.8A GeV, and for a similar centrality class, parametrised by $\langle A_{part}\rangle_b = 37.5$ [26].

4.4 K^-/K^+ ratio as function of kinetic energy

The K^-/K^+ ratio has been studied as a function of the kinetic energy of kaons and their rapidity. Studying particle yield ratio offers two advantages [8]. (i) Experimental

Table 2. Parameters of the K^+ and K^- phase space distributions obtained by fitting the E^{kin}_{CM} and ϑ_{CM} projections of eq. (2): a_2 (polar angle anisotropy parameter), $B_{E_{k1}..E_{k2}}$ (normalisation parameter in eq. (8)), $I_{E_{k1}..E_{k2}}$ (partial integral, see eq. (12)), T_{eff} (effective temperature), and P (total production yield). The first and second error denote the statistical and systematic errors, respectively.

	a_2	$B_{E_{k1}..E_{k2}}$	$I_{E_{k1}..E_{k2}}$	T_{eff} [MeV]	P
K^+	$0.45 \pm 0.08^{+0.18}_{-0.11}$	$[3.2 \pm 0.1^{+0.2}_{-0.5}] \times 10^{-3}$	$[7.35 \pm 0.08^{+0.33}_{-0.73}] \times 10^{-3}$	$109 \pm 2^{+6}_{-13}$	$[3.75 \pm 0.07^{+0.33}_{-0.64}] \times 10^{-2}$
K^-	$0.35 \pm 0.40^{+0.11}_{-0.83}$	$[9.8 \pm 2.1^{+5.0}_{-0.3}] \times 10^{-5}$	$[2.18 \pm 0.21^{+0.30}_{-0.03}] \times 10^{-4}$	$82 \pm 6^{+21}_{-6}$	$[9.5 \pm 1.0^{+2.6}_{-0.1}] \times 10^{-4}$

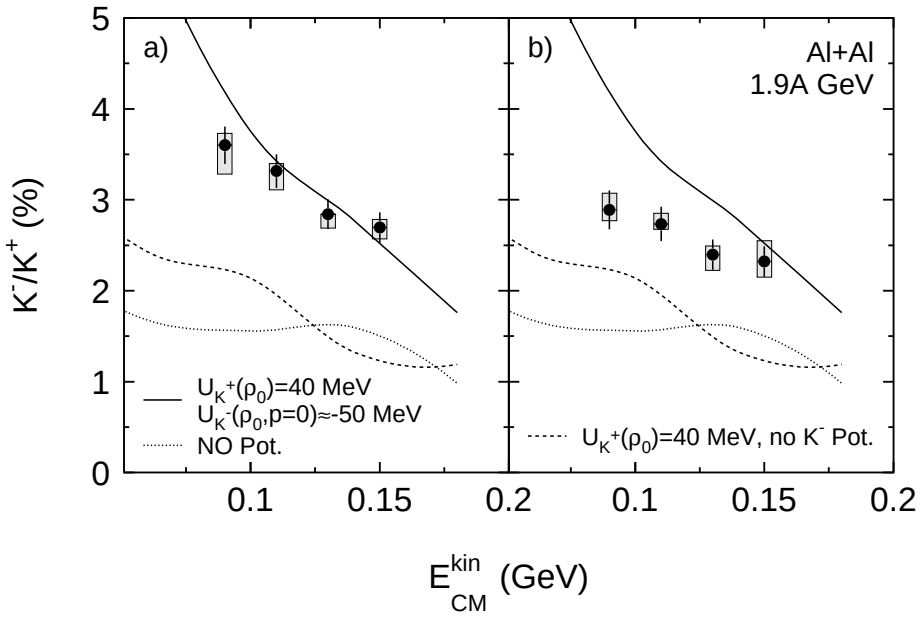

Fig. 9. a) the K^-/K^+ ratio as a function of E^{kin}_{CM} in the Al+Al experiment. Error bars represent the statistical uncertainties. Shaded rectangles represent the estimation of systematic errors. Lines represent the results of HSD model predictions including different values of KN potentials. b) the K^-/K^+ ratio distribution corrected for K^- mesons from ϕ decays. See sec. 6.2 for more details.

biases like detection efficiencies and acceptance losses, are minimised. (ii) In-medium modifications of kaonic properties are predicted to generate the opposite kinematic effects on K^- and K^+, hence the ratio should reveal them more clearly (see sec. 6 for detailed discussion).

Fig. 9a shows the measured K^-/K^+ ratio as a function of the kinetic energy in the c.m. reference frame (E^{kin}_{CM}) for the Al+Al collisions. The polar-angle range $136° < \vartheta_{CM} < 150°$ has been chosen in order to reduce the edge effects of the CDC+Barrel subsystem and provide the largest possible scope of E^{kin}_{CM}. The black points indicate the experimental data. The error bars represent the statistical uncertainties, and the shaded rectangles depict the range of systematic errors. The ratio has been found to decrease with energy E^{kin}_{CM}, which is a direct consequence of the lower transverse slope for K^- compared to that of K^+. A comparison of this distribution with HSD transport model predictions is discussed in sec. 6.

5 Results on ϕ mesons

A sample of about 108 ϕ mesons is too small for a detailed analysis of phase space of this particle. In order to obtain the emission yield in the K^+K^- channel the events were summed up over the available phase space region, and divided by the detection efficiency reported in sec. 3.4.2. The total yield per triggered event was obtained by dividing the result above by the branching ratio of the $\phi \to K^+K^-$ channel, and was found to be:

$$P(\phi) = [3.3 \ \pm \ 0.5 \ (\text{stat}) \ ^{+0.4}_{-0.8} \ (\text{syst})] \times 10^{-4} \quad . \quad (14)$$

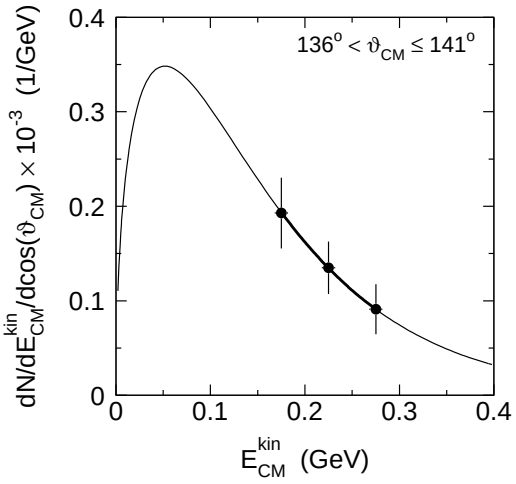

Fig. 10. Kinetic energy distribution of ϕ mesons emitted in polar angles $\vartheta_{\rm CM} \in [115^\circ, 145^\circ]$. The full line depicts the Boltzmann function fit.

The systematic errors include different selection criteria for good tracks, CDC+Barrel matching criteria, and widths of ellipse mass cuts. They also account for the variations of parameters of the ϕ meson emission source assumed in the efficiency simulations, of the invariant mass range used for the normalisation of background, and cuts on charged particle multiplicities used for the collision centrality determination. As before, the systematic errors aim to cover all the observed range of the yield values due to variations of the above-mentioned parameters. The result seems to be slightly higher than the yield of $(2.6 \pm 0.7) \times 10^{-4}$ obtained for the Ar+KCl collisions (although within 0.7 standard deviation they could be equal), at a very similar $\langle A_{\rm part} \rangle_{\rm b}$, but at lower incident energy 1.756A GeV [13]. The obtained yield also seems to be lower than $(4.4 \pm 0.7) \times 10^{-4}$ measured for Ni+Ni collisions at the same beam kinetic energy of 1.91A GeV, but at slightly higher $\langle A_{\rm part} \rangle_{\rm b}$ (although within 1.5 standard deviation both results could be equal) [15].

The kinetic energy distribution was also investigated. To minimise the side effects at the edges of the ToF Barrel detector, the acceptance window was trimmed by requiring $115^\circ < \vartheta_{\rm CM} < 145^\circ$. Fig. 10 shows the measured spectrum. Eq. (10) was fitted to this spectrum, and the inverse slope was found to be:

$$T_{\rm eff} = 93 \pm 14\ ({\rm stat})^{+17}_{-15}({\rm syst})\ {\rm MeV} \quad , \qquad (15)$$

where the systematic errors include the same contributions as for the total ϕ meson yield. The obtained slope seems to be slightly higher than that for the ϕ mesons from the Ar+KCl collisions, 84 ± 8 MeV, and slightly lower than the slope for the Ni+Ni collisions, 106 ± 18 MeV (although in both cases the standard deviation is 0.6).

5.1 Influence of ϕ meson decays on the total K^- yield

The yields of ϕ and K^- mesons for this colliding system are of the same order of magnitude, and their ratio was deduced to:

$$\frac{{\rm P}(\phi)}{{\rm P}({\rm K}^-)} = 0.34 \pm 0.06({\rm stat})^{+0.04}_{-0.14}({\rm syst}) \quad . \qquad (16)$$

The systematic errors were calculated as in the previous subsection, additionally taking into account that each of tested cases of event and track selections was applied simultaneously in the evaluation procedures of the ϕ and K^- yields. This result is found to be similar to the case of the Ar+KCl collisions ($37 \pm 13\%$), and the Ni+Ni case ($44 \pm 7\%$), however, different from the value of about unity observed for the elementary pp collisions at 2.65–2.85 GeV [27,28]). Taking into account the $\phi \rightarrow {\rm K}^+{\rm K}^-$ branching ratio of 48.9%, the result above means that $\left(17 \pm 3^{+2}_{-7}\right)\%$ of emitted K^- mesons originate from ϕ meson decays. To sum up, it appears that in the collisions of heavy-ions at beam energies of 1.7-1.9A GeV the $\phi/{\rm K}^-$ ratio is about 40%, and thus the contribution of ϕ decays into the K^- emission yield of about 20% is a general observation. The influence of the ϕ mesons on the kaon dynamics will be discussed further in sec. 6.2.

6 Discussion

Within the framework of transport models like IQMD or HSD [21,30], it is established that the initial kinematic distributions of $K^{\pm}$ mesons are modified by the interplay between re-scattering, absorption (mostly affecting K^-) and in-medium modification of kaonic properties by the KN potential in dense medium.

According to the IQMD and HSD calculations performed for heavy-ion collisions at 1-2A GeV, the first mechanism should increase the slopes of the kinetic energy distributions of kaons of both signs. Absorption, by filtering out more K^- mesons with lower momenta, should effectively rise the slope, while the KN potential should accelerate K^+, and decelerate K^- [6]. The calculations within the transport models agree with the general experimental finding of superiority of T_{K^+} over T_{K^-} inverse slopes, also observed for the Al+Al system (c.f. eq. (11)).

Generally, it has been shown that transport models are able to describe the kaon (and hyperon) yields and spectra when incorporating the in-medium modifications of kaon properties [6]. Often the mass shifts of kaons in the medium are modelled inside transport codes by applying a parametrisation of the mass as a function of density. This approach is used in HSD for K^+ mesons, while K^- mesons are treated as off-shell particles using the G-Matrix formalism [31].

6.1 K^-/K^+ ratio compared to the HSD model

It has been demonstrated that the ratio of kinetic energy distributions of K^- to K^+ mesons is sensitive to KN potentials calculated within the transport models [8,32,33,34,35]. Fig. 9a shows this ratio for the central Al+Al collisions. The ratio was investigated within the HSD model [30]. The profile obtained without any in-medium effects is shown as dotted line in fig. 9, and falls far off the experimental data both in terms of slope and yield. If only K^+N potential with a linear dependence on density with $U_{K^+N}(\rho_0) = 40$ MeV is included in the calculations, the resulting profile falls slightly closer to the experimental data, as shown by the dashed line, but the agreement is still not reached. Finally, switching the in-medium effects for both kaons and antikaons ($U_{K^+N}(\rho_0) = 40$ MeV and $(U_{K^-N}(\rho_0, p = 0) \approx -50$ MeV) results in the profile depicted by the solid line, reproducing the experimental profile. Thus, a comparison of our data to the transport model predictions leads qualitatively to the same conclusion as obtained in the central Ru+Ru/Zr collisions at 1.69A GeV, and Ni+Ni collisions at 1.93A GeV [8].

However, in the transport models mentioned above the influence of ϕ meson decays is missing (IQMD) or underestimated (HSD). In the following subsection we present an estimation of the range of this influence from the experimental Al+Al data.

6.2 Influence of ϕ mesons on the kaon dynamics

As shown in sec. 5.1, the K^- emission has (at least) two distinct contributions. While negative kaons emitted directly from the collision zone (dubbed below as "direct") reflect the conditions therein, and may carry signatures of modifications of their properties in medium, most K^- mesons from ϕ meson decays are produced outside the collision zone, at $\rho = 0$. As m_ϕ is only 32 MeV larger than $m_{K^+} + m_{K^-}$, the pair of kaons originating from the ϕ meson decay receives only a small portion of energy from the energy balance, and K^- takes only half of this energy. It is therefore natural to expect that the kinematics of these two sources of K^- emission is different. On the other hand, as the yield of K^+ is much higher to that of K^- the influence of ϕ meson decays on these particles is negligible.

In order to find the inverse slope of kinetic energy spectrum of negative kaons emitted from ϕ meson decays, the latter were generated using the PLUTO code [36]. Their emission was simulated according to the Boltzmann distribution with temperature as reported in eq. (15), where statistical and systematic uncertainties were taken into account. ϕ mesons were further permitted to decay into the K^+K^- pairs. The obtained E^{k}_{CM} distribution of K^- mesons was fitted with the Boltzmann function and the inverse slope was found to be:

$$T_{\mathrm{eff},\,K_\phi} = 55.5 \pm 7.1(\mathrm{stat})^{+8.5}_{-7.7}(\mathrm{syst})\,\mathrm{MeV} \quad . \qquad (17)$$

The influence of binning of the energy spectra of particles involved did not change the result significantly.

The inverse slope obtained in this way is clearly lower than that extracted from the inclusive fit to the K^- energy spectrum, c.f. eq. (11). As in the investigated colliding system about 17% of produced K^- mesons originate from the decays of ϕ, one can put forward the hypothesis that the inverse slope of the direct kaons should be greater than the inclusive value. It would imply that the feeding of negative kaons by ϕ meson decays is co-responsible for enhancing

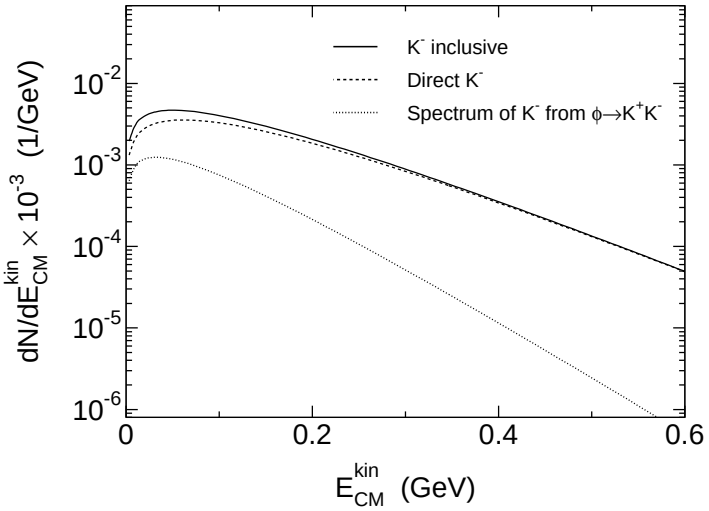

Fig. 11. Kinetic energy distributions of K^- mesons obtained by the inclusive fit to the experimental data (solid line), K^- from ϕ meson decays (dotted line), and "direct" K^- mesons generated from the thermal source (dashed line). See text for details.

the gap between the inverse slopes of K^- and K^+ energy spectra (eq. (11)). A qualitative support for this reasoning was found in Ar+KCl collisions at 1.76A GeV [14], and Ni+Ni collisions at 1.91A GeV [15]. In order to verify this hypothesis, a double-source model of K^- emission from the investigated collision system was constructed. It was assumed that:

- the inclusive K^- emission spectrum is isotropic (an assumption justified by the value of the a_2 parameter comparable to 0 within 1 standard deviation), and described by the Boltzmann distribution with the parameter $T_{\mathrm{eff,\,K^-}}$ (c.f. eq. (17)), and the normalisation factor shown in eq. (13).
- K^- mesons originating from ϕ meson decays and observed in the experiment are produced outside the collision zone. (Some ϕ mesons decay inside this zone, but the modifications of their momenta in course of the final state interactions, or the absorption effect, especially affecting K^-, may cause such events not to be reconstructable. This argument implies, of course, some simplifications.)
- both the "direct" and the ϕ meson sources of K^- are characterised by the Boltzmann distributions, with parameters: $T_{\mathrm{eff,\,K_{direct}}}$ (unknown, to be found), $T_{\mathrm{eff,\,K_\phi}}$ (c.f. eq. (17)), and the normalisation factors weighting the inclusive K^- emission probability according to the found ϕ/K^- ratio (cf. eq. (16)).

Fig. 11 shows the total kinetic energy distribution of K^- mesons, and its two respective components. The "direct" component was obtained by subtracting the contribution from the ϕ meson decays from the inclusive spectrum. The Boltzmann function of the form of eq. (10) was fitted to this component and the inverse slope was found to be:

$$T_{\mathrm{eff,\,K_{direct}}} = 89 \pm 9\ ^{+24}_{-11}\ \mathrm{MeV} \quad . \tag{18}$$

The uncertainties of this result take into account the reported statistical and systematic uncertainties of $P\left(K^-\right)$ and $T_{\mathrm{eff,\,K^-}}$, and of the parameters characterising the ϕ meson contribution to the K^- spectrum. Judging from the raw values, the inverse slope parameter of the "direct" antikaons (89 MeV) seems to be (somewhat) higher than the inclusive value (82 MeV), although not as high as the slope for the K^+ (109 MeV).

In a previous subsection the experimentally obtained K^-/K^+ ratio as function of the kinetic energy was compared to the HSD model calculations, in order to draw conclusions on the strength of the KN interaction. ϕ meson production is included in the HSD model and contributes to the K^- production. But the predicted yield of ϕ's is about 5-10 times lower than the measured one, and the contribution of ϕ decays to the K^- spectra is assumed to be negligible for the following discussion [37]. Within the double-source model of K^- meson emission, one can now substitute the "direct" K^- component only (instead of the inclusive yield), as shown in fig. 9b. One can find, that this subtraction results in some flattening and lowering of the K^-/K^+ distribution profile. One can still uphold the statement that the calculations without

the in-medium modifications of kaonic properties does not describe the data. However, it seems that the value of the K^-N potential applied in the HSD calculations should be somewhat lower to reproduce the experimental pattern.

7 Summary

FOPI has investigated the production yields and phase space distributions of K^+, K^-, and ϕ mesons from central collisions of Al+Al at a beam kinetic energy of 1.9A GeV. The anisotropy parameters of the angular distributions, $a_2 = 0.45 \pm 0.08^{+0.18}_{-0.11}$ for K^+, and a_2 consistent with 0 for K^- were found to be in line with the findings from the central Ni+Ni collisions at the same beam energy. Also, the inverse slopes of kaons ($T_{\rm eff}(K^+) = 109 \pm 2^{+\ 6}_{-13}$ MeV, and $T_{\rm eff}(K^-) = 82 \pm 6^{+21}_{-\ 6}$ MeV), and their total production yields per triggered event ($P_{K^+} = \left[3.75 \pm 0.07^{+0.33}_{-0.64}\right] \times 10^{-2}$, and $P_{K^-} = \left[0.95 \pm 0.10^{+0.26}_{-0.01}\right] \times 10^{-3}$) were found to be consistent with the previously accumulated systematics, and in agreement with the well established effect of superiority of $T(K^+)$ over $T(K^-)$. A comparison of the measured K^-/K^+ ratio as function of kinetic energy to the HSD transport model calculations (a version with the negligible ϕ meson production) suggests that the scenario of in-medium KN potentials ($U_{K^+N}(\rho_0) = 40$ MeV, and $U_{K^-N}(\rho_0, p = 0) \approx -50$ MeV) is favoured over the one without the in-medium effects.

The emission of ϕ mesons was investigated in their K^+K^- decay channel. The production yield was found to be $\left[3.3 \pm 0.5^{+0.4}_{-0.8}\right] \times 10^{-4}$, and the inverse slope of the kinetic energy distribution $T_{\rm eff} = 93 \pm 14^{+17}_{-15}$ MeV. While the contribution of the ϕ decay channel into charged kaons to K^+ meson emission is negligible, the kaons originating from ϕ-mesons were found to constitute $(17 \pm 3^{+2}_{-7})\%$ of the total K^- yield, a fraction sufficient to consider while drawing physical conclusions from distributions of kinematic observables involving K^-. Therefore, the two-source model of K^- emission (the "direct" component from the collision zone, and the daughter kaons from ϕ decays) was applied to the kinetic energy spectrum of K^-. The inverse slope of the "direct" component was estimated to be $T_{\rm eff,\,K_{direct}} = 89 \pm 9\ ^{+24}_{-11}$ MeV. The K^-/K^+ ratio after removal of the ϕ contribution was found to appear somewhat smaller and more flattened out as function of kinetic energy, which suggests that the in-medium effects parametrised by the U_{K^-N} potential could be weaker.

Acknowledgements

This work was supported by the German BMBF under Contract No. 05P12VFHC7, Korea Science and Engineering Foundation (KOSEF) under Grant No. F01-2006-000-10035-0, by the mutual agreement between GSI and IN2P3/CEA, by the Polish Ministry of Science and Higher Education under Grant No. DFG/34/2007, by the National Science Centre in Poland under Grant No. 2011/03/B/ST2/03694, by the Hungarian OTKA under Grant No. 47168, within the Framework of the WTZ program (Project RUS 02/021), by DAAD (PPP D/03/44611), and by DFG (Projekt 446-KOR-113/76/04 and 436 POL 113/121/0-1). We have also received support by the European Commission under the 6th Framework Program under the Integrated Infrastructure on: Strongly Interacting Matter (Hadron Physics), Contract No. RII3-CT-2004-506078.

References

1. G.E. Brown, and M. Rho, Phys. Rev. Lett. **66**, 2720 (1991).
2. W. Weise, Nucl. Phys. A **610**, 35c (1996).
3. T. Waas, M. Rho, and W. Weise, Nucl. Phys. A **617**, 449 (1997).
4. M.F.M. Lutz, Prog. Part. Nucl. Phys. **53**, 125 (2004), doi:10.1016/j.ppnp.2004.02.008.
5. C. Fuchs, Prog. Part. Nucl. Phys. **56**, 1 (2006), doi:10.1016/j.ppnp.2005.07.004.
6. C. Hartnack, H. Oeschler, Y. Leifels, E.L. Bratkovskaya, and J. Aichelin, Phys. Rep. **510**, 119 (2012), doi:10.1016/j.physrep.2011.08.004.
7. J. Schaffner-Bielich, J. Bondorf, I. Mishustin, Nucl. Phys. A **625**, 325 (1997), doi:10.1016/S0375-9474(97)81464-9.
8. K. Wiśniewski *et al.*, Eur. Phys. J. A **9**, 515 (2000), doi:10.1007/s100500070008.
9. A. Förster *et al.*, Phys. Rev. C **75**, 024906 (2007), doi:10.1103/PhysRevC.75.024906.
10. M.L. Benabderrahmane *et al.*, Phys. Rev. Lett. **102**, 182501 (2009), doi:10.1103/PhysRevLett.102.182501.
11. G. Agakishiev *et al.*, Phys. Rev. C **82**, 044907 (2010), doi:10.1103/PhysRevC.82.044907.
12. V. Zinyuk *et al.*, Phys. Rev. C **90**, 025210 (2014), doi:10.1103/PhysRevC.90.025210.
13. G. Agakishiev *et al.*, Phys. Rev. C **80**, 025209 (2009), doi:10.1103/PhysRevC.80.025209.
14. M. Lorenz, PoS (BORMIO 2010), 038.
15. K. Piasecki *et al.*, Phys. Rev. C **91**, 054904 (2015), doi:10.1103/PhysRevC.91.054904.

16. J. Ritman, Nucl. Phys. (Proc. Suppl.) B **44**, 708 (1995).
17. B. Sikora, Acta Phys. Pol. B **31**, 135 (2000).
18. J. Gosset *et al.*, Phys. Rev. C **16**, 629 (1977), doi:10.1103/PhysRevC.16.629.
19. K.A. Olive *et al.* (Particle Data Group), Chin. Phys. C **38**, 090001 (2014), doi:10.1088/1674-1137/38/9/090001.
20. wwwasdoc.web.cern.ch/wwwasdoc/geant_html3/geantall.html
21. C. Hartnack *et al.*, Eur. Phys. J. A **1**, 151 (1998), doi:10.1007/s100500050045.
22. A. Mangiarotti *et al.*, Nucl. Phys. A **714**, 89 (2003), doi:10.1016/S0375-9474(02)01366-0.
23. E. Schnedermann, J. Sollfrank, and U. Heinz, Phys. Rev. C **48**, 2462 (1993).
24. X. Lopez *et al.*, Phys. Rev. C **81**, 061902(R) (2010), doi:10.1103/PhysRevC.81.061902.
25. M. Menzel *et al.*, Phys. Lett. B **495**, 26 (2000), doi:10.1016/S0370-2693(00)01232-6.
26. R. Barth *et al.*, Phys. Rev. Lett. **78**, 4007 (1997), doi:10.1103/PhysRevLett.78.4007.
27. F. Balestra *et al.*, Phys. Rev. C **63**, 024004 (2001), doi: 10.1103/PhysRevC.63.024004.
28. Y. Maeda *et al.*, Phys. Rev. C **77**, 015204 (2008), doi: 10.1103/PhysRevC.77.015204.
29. B. Borasoy, R. Nißler, and W. Weise, Eur. Phys. J. A **25**, 79 (2005), doi: 10.1140/epja/i2005-10079-1.
30. W. Cassing *et al.*, Phys. Rep. **308**, 65 (1999), doi:10.1016/S0370-1573(98)00028-3.
31. W. Cassing, L. Tolós, E.L. Bratkovskaya, A. Ramos, Nucl. Phys. A **727**, 59 (2003), doi:10.1016/S0375-9474(96)00461-7.
32. A. Förster *et al.*, Phys. Rev. Lett. **91**, 152301 (2003), doi: 10.1103/PhysRevLett.91.152301.
33. G.Q. Li, G.E. Brown, Phys. Rev. C **58**, 1698 (1998), doi:10.1103/PhysRevC.58.1698.
34. W. Cassing *et al.*, Nucl. Phys. A **614**, 415 (1997), doi:10.1016/S0375-9474(96)00461-7.
35. C. Hartnack, H. Oeschler, and J. Aichelin, Phys. Rev. Lett. **90**, 102302 (2003), doi:10.1103/PhysRevLett.90.102302.
36. I. Frohlich et al., PoS ACAT2007, 076 (2007).
37. Y. Leifels (private communication).